Ends and middle: global force balance determines septum location in fission yeast

Xavier Le Goff[1*], Jordi Comelles[2,3,4,5,6], Charles Kervrann[7] and Daniel Riveline[2,3,4,5,6*]

1 Univ Rennes, CNRS, IGDR (Institut de génétique et développement de Rennes) - UMR 6290, F-35000 Rennes, France
2 *Laboratory of Cell Physics ISIS/IGBMC, ISIS & icFRC, Université de Strasbourg & CNRS, 8 allée Gaspard Monge, Strasbourg 67000, France*
3 *Institut de Génétique et de Biologie Moléculaire et Cellulaire, Illkirch, France*
4 *Centre National de la Recherche Scientifique, UMR7104, Illkirch, France*
5 *Institut National de la Santé et de la Recherche Médicale, U964, Illkirch, France*
6 *Université de Strasbourg, Illkirch, France*
7 SERPICO Team, INRIA Rennes, Campus de Beaulieu 35042 Rennes, France

*To whom correspondence should be addressed: xavier.le-goff@univ-rennes1.fr, riveline@unistra.fr

Abstract

The fission yeast cell is shaped as a very regular cylinder ending by hemi-spheres at both cell ends. Fission yeast cells elongate during interphase keeping this regular shape, set by a balance between cell wall stiffness and turgor pressure. The central position of the nucleus is used as a spatial cue to assemble a contractile actomyosin ring at the geometric cell center when cells entered mitosis. This ring is used to drive the synthesis of a specific cell wall structure called the division septum. The septum is ultimately the place where the cell wall undergoes a fracture, leaving two closed daughter cells approximately half the mother cell after cytokinesis. We proposed scaling arguments where the radii of curvatures of cell ends influence constraints on the cell wall. This relation predicts that the division site would be located closer to the cell end with the highest radius of curvature. We decided to test experimentally whether altered shapes of cell end actually correlate with a displaced division site, leading to an asymmetric cell division. Our results show that the division site position depends on the radius of curvatures of both ends.

Introduction

The fission yeast cell is shaped as a very regular cylinder ending by hemi-spheres at both cell ends. Fission yeast cells elongate during interphase keeping this regular shape, set by a balance between cell wall stiffness and turgor pressure [1]. The cell is being remodelled locally at the cell ends to promote cell extension. The nucleus is permanently maintained in the middle of the cell by different forces, including microtubule pushing forces [2,3]. The central position of the nucleus is used as a spatial cue to assemble a contractile actomyosin ring when cells entered mitosis. This ring is built up at the inner cell cortex perpendicular to the long axis of the cell at the geometric cell center. This ring is used to drive the synthesis of a specific cell wall structure called the division septum. This septum physically separates the daughter cells into two cells. The septum is ultimately the place where the cell wall undergoes a fracture, leaving two closed daughter cells approximately half the mother cell after cytokinesis. We proposed scaling arguments where the radii of curvatures of cell ends R_i influence constraints on the cell wall [1]. They ultimately produce an effect on the division site position. This relation predicts that a higher radius of cell end curvature at one cell end should displace the division site by a length L_{shift} due to unbalanced strengths applied on the cell wall. The division site would be located closer to the cell end with the highest radius of curvature. We decided to test experimentally whether altered shapes of cell end actually correlate with a displaced division site, leading to an asymmetric cell division. We combined genetics together with live cell imaging. We used a constitutive deletion *tea4*Δ mutant and a conditional *kin1-as1* mutant These mutations affect the shapes of cell ends. Our results show that the division site position depends on the radius of curvatures of both ends.

Results and Discussion

According to our scaling law, the cell end curvature would impact on cell division site position at the time of septum ingression due to cell wall constraints. Equation 10 of reference [1] showed that this does not depend on the total cell length *L* (Figure 1B) : $l_{shift} = \frac{\gamma}{\Delta P \cdot R} \cdot (R_1 - R_2)$, (Eq. 1), where *R* is the mean radius of the long axis, ΔP the constant difference in pressure between the inside and the outside of the cell and $\gamma$the cell wall surface tension. Therefore, we monitored the cell division site localization using the expression of the cytokinetic ring component Cdc15-GFP (Figure 1). Cellular outlines were stained with the cell wall isolectin-488 label.

First, we compared wild type (WT) and the asymmetrically dividing mutant *tea4*Δ (Figure 1A). The Tea4 protein is involved in bipolar activation of cell growth in the cell ends. *Tea4*Δ cells showed altered cell morphology including one more enlarged cell end than the other and an asymmetrically positioned division site [4,5]. We measured cell end curvatures on both cell ends. Division site position was determined with Cdc15-GFP. The L_{shift} value was calculated as *L/2-a* were L stands for the total cell length and *a* for the shortest distance between the ring and one cell end (cell end1). To calculate the R_1-R_2 value, radii of curvatures were measured as follows: R_1 for cell end1 and R_2 for the other cell end. We observed an increased asymmetry in *tea4*Δ cells compared to WT (Figure 1). On one hand, cell end radii are different in *tea4*Δ cells compared to WT cells. The difference of radii of cell end curvatures (R_1-R_2) slightly increased from 0.13±0.01 µm for WT cells to 0.21±0.02 µm for *tea4*Δ (Figure 2A). On the other hand, the mean value of L_{shift} increased from 0.26±0.05 µm for WT cells to 0.62±0.06 µm for *tea4*Δ (Figure 2A). There is clearly a larger amplitude of L_{shift} in *tea4*Δ cells indicating that *tea4*Δ cells

divide more asymmetrically than WT cells. Finally, the L_{shift}, plotted as a function of the R_1-R_2 difference of radii of cell end curvatures (Figure 1C), showed a positive correlation between L_{shift} and R_1-R_2 for *tea4*Δ cells (Pearson's correlation coefficient 0.72), whereas no correlation was observed for WT cells (Pearson's correlation coefficient 0.07). Therefore, the experimental results show that the division site is displaced towards the end with the highest radius of curvature, which is consistent with our prediction.

*Tea4*Δ cells are constitutively misshapen and cell end curvatures differences may arise from cell wall defects inherited through several generations independently of cell division site selection. Thus, we used *kin1-as1*, a conditional allele of the cell wall regulating Kin1 kinase, that promoted cell division site mispositioning within the duration of a cell division cycle. *Kin1-as1* was inhibited using a small molecule called NMPP1 added into the culture medium [6]. *Kin1*$^-$ (*kin1-as1*+NMPP1) and *kin1*$^+$ (*kin1-as1*+DMSO) cells are isogenic but cultured with or without the inhibitor for 2 hours, respectively. *Kin1*$^-$ cells adopt an asymmetric cell division pattern in less than a generation time (see Figure 1A). We monitored division site position and cell end curvatures using the method described above. A larger L_{shift} is clearly observed in *kin1*$^-$ cells (L_{shift} = 0.57±0.04 μm n=48) compared to *kin1*$^+$ cells (L_{shift} = 0.25±0.02 μm n=35) (Figure 2A). Thus, indicating that *kin1*$^-$ divide more asymmetrically than DMSO treated cells and WT cells. Furthermore, R_1-R_2 value is higher in *kin1*$^-$ cells (0.17±0.02 μm) compared to *kin1*$^+$ cells (0.06 ±0.01 μm), showing that cell end radii are less equivalent (Figure 2B). Again, L_{shift}, plotted as a function of the R_1-R_2 (Figure 1C), showed a positive correlation between L_{shift} and R_1-R_2 for *kin1*$^-$ cells compared to *kin1*$^+$ cells. L_{shift} was again displaced towards the end with the highest radius of curvature, confirming the results with the *tea4*Δ mutant and strongly supporting the scaling laws of paper [1]. Based on these results and Eq. 1, we could extract a quantitative estimate for the wall surface tension γ = 9.7±5.2 Nm (Figure 3), in good agreement with independent methods [7].

Our results show that fission yeast cell end shapes influence the division site position. In WT cells, the small difference in both cell end radii promotes balanced global forces that place the division site close to the geometric cell center. Accordingly, daughter cells divide at nearly equal sizes and this might be crucial for cell population fitness regarding symmetric partitioning of cellular components and damaged material inheritance [8]. We propose that two mechanisms contribute to symmetry of division in fission yeast: an "external" output from cell wall driven forces and an 'internal" output driven by microtubule-dependent nuclear localization. In mutants where the cell wall synthesis machinery is depolarized from cell ends, the external cell wall output exceeds a threshold and cells divide asymmetrically, suggesting that the internal output cannot compensate the defect. The role of cell wall forces proposed here may be a broad mechanism in single celled symmetrically dividing organisms to produce equally sized daughter cells at each cell division.

Experimental procedures

Yeast Strains and General Techniques

S. pombe strains used in this study are XLG52 (*h- cdc15::GFP-ura4⁺ ura4-D18 leu1-32*, a kind gift of V. Simanis, Switzerland), XLG540 (*h- tea4::ura4+ ura4-D18 cdc15::GFP-ura4⁺ leu1-32*), XLG741 (*h- cdc15::GFP-ura4⁺ kin1-as1 leu1-32 ura4-D18*). Growth media and basic techniques for *S. pombe* have been described [9].

Microscopy

A spinning disk Nikon TE2000 microscope, equipped with a 100x 1.45 NA PlanApo oil-immersion objective lens and a HQ2 Roper camera, was used for data acquisition. Cells were expressing the acto-myosin ring component Cdc15-GFP and were stained 10 minutes with isolectin-488 (Molecular probes) that stains the global cell wall (but not the septum). Metamorph software was used for capturing images. The "three point circular" ImageJ Plugin allows to draw a ring with three points at a cell end and it gives the radius of curvature. We used this Plugin to measure radii of curvature to obtain the best measurements. Cell lengths (L, a) were measured with the Plot profile Plugin.

Statistical analyses and graphical representation

Statistical analysis was done using GraphPad Prism. Results are presented as mean ± s.e.m of N = 3 experiments, n_{WT} = 52 cells, $n_{tea4\Delta}$ = 51 cells, $n_{kin1\text{-}as1+DMSO}$ = 35 cells and $n_{kin1\text{-}as1+NMPP1}$ = 48 cells. First, normality of the datasets was tested by the d'Agostino-Pearson normality test. Statistical differences were analyzed by t-test (Gaussian distribution) and Mann-Whitney test (non Gaussian distribution). The Pearson r correlation coefficient was used in order to test the relation between $(R_1\text{-}R_2)$ and L_{shift} for all the conditions. $(R_1\text{-}R_2)$ as function of L_{shift} were fitted using a linear regression. To obtain the surface tension γ for *tea4*Δ cells. γ was calculated according to equation 1 assuming $\Delta P = 0.85$ MPa for every cell. The distribution of γ was plotted and fitted with a Gaussian distribution $y = y0 + A\cdot\exp(-(x-x_c)^2/(2\cdot w^2))$, where x_c is the mean value for γ and w corresponds to the standard deviation.

Acknowledgments

This work was supported by a grant for "Aide aux financements de projets innovants interdisciplines" from the SFR BIOSIT (UMS CNRS 3480 - US INSERM 018, Rennes, France) to XLG, Unistra and CNRS funds to DR. We thank J.R. Paulson and X. He (Oshkosh University, USA) for providing the NMPP1, the MRic microscopy platform for fluorescence microscopy equipment at the SFR BIOSIT (Rennes, France), F. Chang (San Francisco, USA) and V. Simanis (Lausanne, Switzerland) for strains, J. Pécreaux (IGDR, Rennes, France) and A. Trubuil (INRA, Jouy-en-Josas, France) for their help in initial image analyses and Y. Arlot-Bonnemains (IGDR, Rennes, France) for support.

References

1) Riveline, D. (2009). Explaining lengths and shapes of yeast by scaling arguments. PLoS One, 4(7), e6205.
2) Tran, P.T., Marsh, L., Doye, V., Inoué, S. and Chang, F. (2001). A mechanism for nuclear positioning in fission yeast based on microtubule pushing. J. Cell Biol. 16, 397-411.
3) Daga, R.R. and Chang, F. (2005). Dynamic positioning of the fission yeast cell division plane. Proc Natl Acad Sci U S A 102(23), 8228-8232.
4) Tatebe, H., Shimada, K., Uzawa, S., Morigasaki, S. and Shiozaki, K. (2005). Wsh3/Tea4 is a novel cell-end factor essential for bipolar distribution of Tea1 and protects cell polarity under environmental stress in S. pombe. Curr Biol. 15(11), 1006-1015.
5) Martin, S.G., McDonald, W.H., Yates, J.R. 3rd and Chang, F. (2005). Tea4p links microtubule plus ends with the formin for3p in the establishment of cell polarity. Dev Cell. 8(4), 479-491.
6) Cadou, A., Couturier, A., Le Goff, C., Soto, T., Miklos, I., Sipiczki, M., Xie, L., Paulson, J.R., Cansado, J. and Le Goff, X. (2010). Fission yeast Kin1 is a plasma membrane-associated kinase which regulates the cell surface. Mol. Microbiol. 77(5), 1186-1202.
7) Minc, N., Boudaoud, A. and Chang, F. (2009). Mechanical Forces of Fission Yeast Growth. Curr Biol, 19, 1096–1101.
8) Coelho, M., Lade, S.J., Alberti, S., Gross, T. and Tolić, I.M. (2014). Fusion of protein aggregates facilitates asymmetric damage segregation. PLoS Biol. 12(6), e1001886.
9) Moreno, S., Klar, A., and Nurse, P. (1991) Molecular genetic analysis of fission yeast Schizosaccharomyces pombe. Methods Enzymol, 194, 795-823.

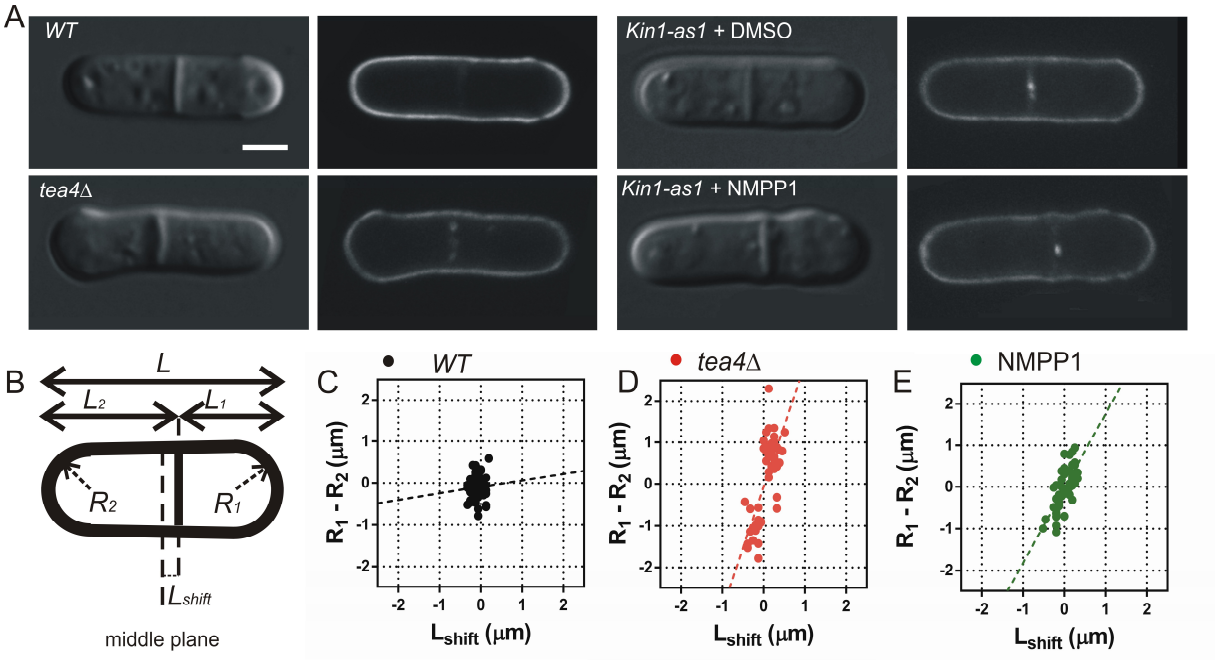

Figure 1. *a) DIC (left) and fluorescent (right) microscopy images (cdc15-GFP, isolectin-488) of WT, tea4Δ, kin1-as1+DMSO and kin1-as1+NMPP1 cells, Scale bar 2μm.* ***b)*** *Schematics of the parameters measured in each cell: R_i corresponds to the radii of curvature at the cell "end i", and L_i corresponds to the distance between "end i" and septum; L_{shift} is defined as the distance between the septum and the middle plane ($L_{shift}=(L_2-L_1)/2$, L the total length).* ***c)*** *Correlation between L_{shift} and R_1-R_2 for the different mutants. The fits of Equation 1 are shown in the graphs. $n_{WT}=52$, $n_{tea4\Delta}=51$ $n_{Kin1\text{-}as1+DMSO}=35$ and $n_{Kin1\text{-}as1+NMPP1}=48$. Pearson's correlation coefficients are 0.07, 0.72 and 0.72 respectively.*

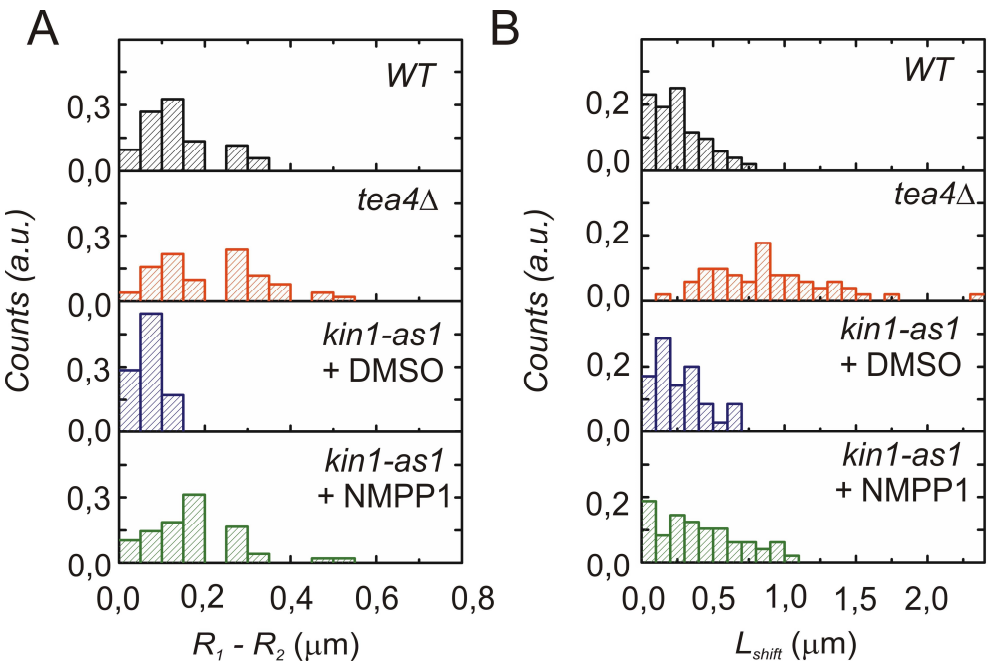

Figure 2. *Distributions of the absolute values of R_1-R_2 (**A**) and L_{shift} (**B**) for the different conditions. R_1-R_2 distributions are statistically different for WT and tea4Δ (t-test, p = 0.0003) and for kin1-as1 DMSO and NMPP1 (Mann-Whitney, p < 0.0001). L_{shift} distributions are statistically different for WT and tea4Δ (Mann-Whitney, p < 0.0001) and for kin1-as1 DMSO and NMPP1 (t-test, p = 0.0122). N = 3 experiments, n_{WT} = 52 cells, $n_{tea4\Delta}$ = 51 cells, $n_{kin1\text{-}as1+DMSO}$ = 35 cells and $n_{kin1\text{-}as1+NMPP1}$ = 48 cells.*

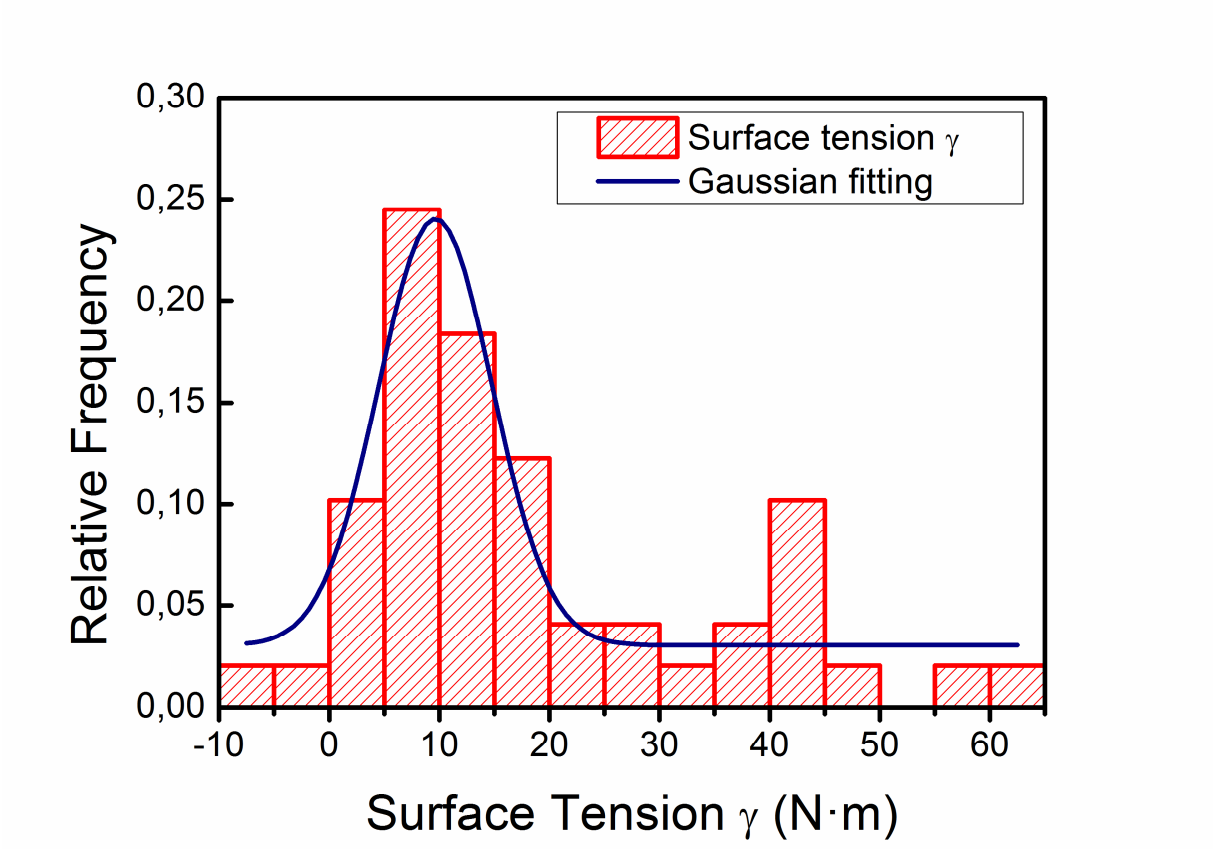

Figure 3. *Distribution of surface tension γfor tea4Δ cells. γwas calculated according to Equation 1 assuming ΔP = 0.85 MPa [7]. The data were fitted assuming a Gaussian distribution, obtaining a value for the surface tension of γ= 9.7 ± 5.2 N·m.*